Bulletin of the Seismological Society of America, Vol. 97, No. 5, pp. 1607–1620, October 2007, doi: 10.1785/0120060236

Subsidence, Compaction, and Gravity Sliding: Implications for 3D Geometry, Dynamic Rupture, and Seismic Hazard of Active Basin-Bounding Faults in Southern California

by Craig Nicholson, Marc J. Kamerling, Christopher C. Sorlien, Thomas E. Hopps, and Jean-Pierre Gratier

Abstract In southern California, high rates of measured geodetic shortening occur where active basin-bounding faults thrust early-Cenozoic rocks over young unconsolidated sediments. This implies that compaction, subsidence, and other nonelastic processes of footwall deformation may play an important role in contributing to the high rates of observed crustal strain. Even in the absence of active tectonic shortening, sediment compaction alone can produce surficial motions that mimic deep fault slip or elastic strain accumulation. Differential compaction and subsidence of footwall sediments relative to hanging-wall rocks can lead to increased vertical separation, basinward collapse, and fault rotation about horizontal axes. Such effects contribute to net horizontal and vertical motions in both geologic and geodetic data, and—if not properly accounted for—result in incorrect estimates of the inferred seismic hazard.

Subsidence and compaction also increase the potential for gravity sliding toward the basin and the development of significant nonplanar 3D fault geometry. A prime example occurs along the San Cayetano fault that bounds the eastern Ventura basin. At shallow levels, a large thrust sheet (the Modelo Lobe) with low dip extends out in front of the more steeply dipping, planar fault segment by over 4 km, is nearly 2 km thick, and occupies over 60 cubic km. This geometry is strongly indicative of gravity-driven failure resulting from hanging-wall uplift, basinward tilt, and collapse, enhanced by footwall subsidence and compaction. Failure of this mega-slide off the hanging-wall block most likely occurred within the Rincon Formation, a thick ductile shale sequence that often accommodates detachment slip. This 3D geometry has significant implications for how the fault may behave during dynamic rupture and implies that additional care should be taken in extrapolating near-surface measurements or estimates of fault slip and dip to seismogenic depths.

Introduction

The western Transverse Ranges of southern California are one of the most active tectonic regions in the world. Geologic and geodetic data indicate that both the Los Angeles and Ventura basins currently accommodate high rates of oblique crustal shortening (e.g., Donnellan *et al.*, 1993; Yeats, 1993; Huftile and Yeats, 1995; Hager *et al.*, 1999; Argus *et al.*, 1999, 2005) including components of regional tectonic rotation. Active convergence and rapid subsidence across the Ventura basin have produced uplift rates that exceed 10 mm/yr and one of the thickest sections of Plio-Pleistocene strata ever found (Yeats *et al.*, 1994). Significant amounts of oblique convergence (up to 7 mm/yr) have been documented across the eastern Santa Barbara Channel (Larsen *et al.*, 1993). The 1994 *M* 6.7 Northridge earthquake occurred on a blind, south-dipping fault beneath the San Fernando Valley that is considered part of the active fault and fold system that extends westward into the Ventura basin and eastern Santa Barbara Channel (Fig. 1) (Yeats and Huftile, 1995). High rates of crustal shortening and volumetric strain change are also observed in the northern Los Angeles basin (Bawden *et al.*, 2001; Argus *et al.*, 2005), where the highest gradients in crustal motion are typically localized across basin-bounding faults. This deformation—observed geologically and measured geodetically—is inferred to represent a significant seismic hazard (Dolan *et al.*, 1995; U.S. Geological Survey, 1998), as it is presumed to reflect the

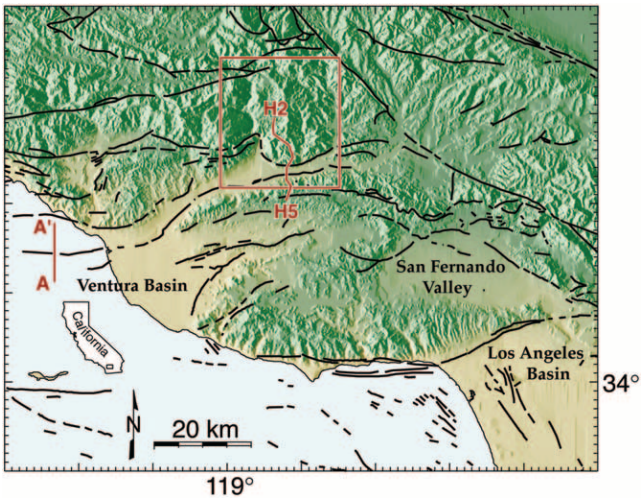

Figure 1. Location map showing shaded topography and major mapped faults (black lines) of portions of the central and western Transverse Ranges, California. Box outlines area of shaded digital elevation model (DEM) with overlaid geology shown in Figure 11. Locations of correlation cross section, H2–H5 (Fig. 2) and seismic-reflection profile, AA′ (Fig. 4) are also shown.

accumulation and release of elastic strain across a series of active faults and fault-related folds.

Understanding this deformation and the complex system of faults by which this deformation occurs is inherently a 3D problem. However, many models used to infer subsurface fault geometry, or used to resolve geodetic strain or geologic data into fault slip are 2D, and typically presume rigid footwall blocks, nondeforming planar fault surfaces, and deformation that is largely restricted to the hanging wall (e.g., Suppe and Medwedeff, 1990; Namson and Davis, 1991; Donnellan *et al.*, 1993; Shaw and Suppe, 1994, 1996; Hager *et al.*, 1999; Bawden *et al.*, 2001; Argus *et al.*, 2005). In California though, deep, subsiding basins (like Ventura and Los Angeles) are often bounded by oblique reverse faults that thrust early-Cenozoic and older rocks over young unconsolidated sediments. Figure 2 is a vertical correlation structure cross section across the Ventura basin (Hopps *et al.*, 1992) and clearly shows how the much older, more consolidated Sespe Formation (red, ~30 Ma [Howard, 1988]) has been uplifted and emplaced above the much younger, less consolidated, and relatively undeformed Saugus Formation (yellow, ~500 ka [Yeats, 1993]) by the north-dipping San Cayetano thrust fault. The figure also documents the collapse and rotation of the shallow San Cayetano and Oak Ridge faults about horizontal axes toward the basin. Because most tectonic models alone would have considerable difficulty in explaining the development of such significant nonplanar 3D fault surfaces, this suggested to us that basin subsidence, compaction, and other nonelastic processes of footwall deformation may play an important role in accommodating regional tectonic strain and in helping to produce the observed rotated and nonplanar geometry of these basin-bounding faults.

In this article, we discuss these nonelastic effects and their possible contributions to measurements of geodetic strain and the development of nonplanar fault surfaces. The influence of gravitational potential energy release and megasliding off the uplifting hanging-wall block and onto the footwall is also considered, in particular for the San Cayetano fault. The resulting complex 3D fault geometry has significant implications for how fault slip is resolved, how the fault may behave during dynamic earthquake rupture, and how this may affect the assessment of seismic hazard.

Data and Observations

Defining Subsurface Structure, Stratigraphy, and 3D Fault Surfaces

To better understand the nature of this ongoing deformation, we developed an integrated, geologic/geophysical database of active 3D fault and fold structure for the Ventura basin and eastern Santa Barbara Channel. This database includes industry well logs, surface geologic maps, seismic-reflection data, correlation cross sections, subsurface structure contour maps, digital topography, velocity studies, and detailed analysis of the local seismicity (Nicholson and Kamerling, 1998, 1999; Sorlien *et al.*, 2000). Within the onshore portion of the Ventura basin, there are an estimated 14,000 drill holes. Subsurface information from these wells can include velocity, electric, resistivity, porosity, and density logs, as well as lithologic, paleontologic, and dipmeter data. Numerous wells and extensive grids of high-quality industry multichannel seismic (MCS) reflection data also exist offshore (Ogle *et al.*, 1987; Redin *et al.*, 1998, 2005; Childs and Hart, 2004). Over a 5-year period, the Ventura Basin Study Group (VBSG) (Hopps *et al.*, 1992) conducted a systematic study of the subsurface structure and stratigraphy within the onshore basin. This study consisted of a detailed, integrated analysis of nearly 1200 deep-penetration (1–5 km) correlated wells. Many of these wells drill active fault and fold structures associated with major fault systems, including the San Cayetano, Oak Ridge, and Santa Susana faults (e.g., Fig. 2), and in several cases, have sufficient fault-penetration coverage to uniquely define shallow subsurface 3D fault geometry (Fig. 3) (Çemen, 1989; Hopps *et al.*, 1992). Images of VBSG structure maps and cross sections are available at http://projects.crustal.ucsb.edu/hopps.

Further confirmation of subsurface structure and fault geometry is provided by integrating seismicity, topography, and deep-penetration MCS reflection data. For example, Figure 4 shows an interpreted, industry MCS reflection line across the offshore Oak Ridge fault in the eastern Santa Barbara Channel (Kamerling and Nicholson, 1996). Note that without proper lithologic, age, depth, and dip control provided by offshore wells, few of the important geologic features of the subsurface structure could be derived from in-

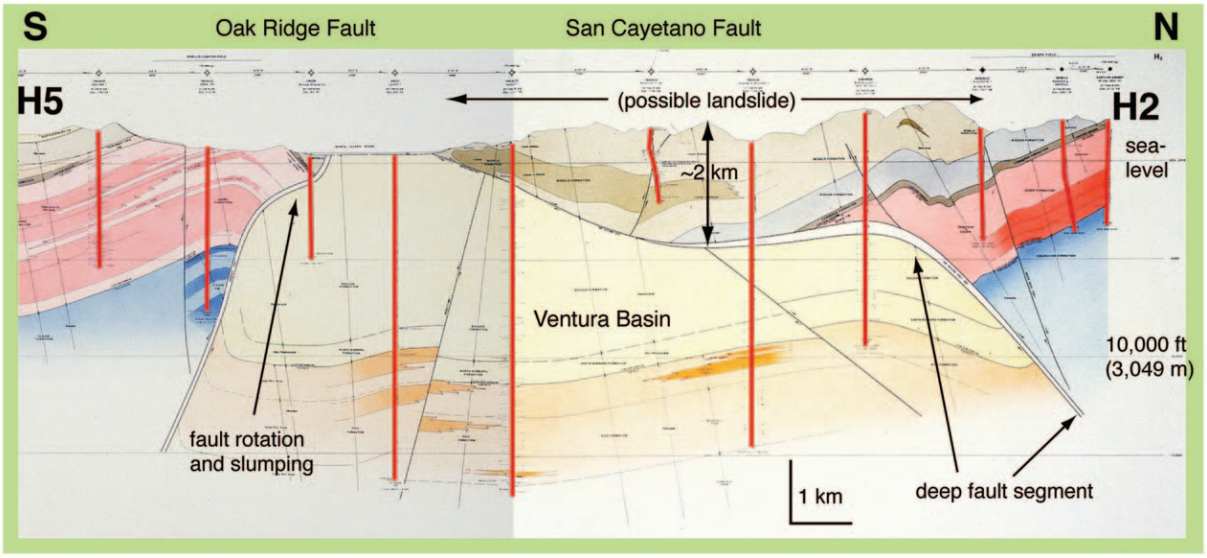

Figure 2. Vertical structure cross section (H2–H5) across Ventura basin and both the Oak Ridge and San Cayetano faults (Hopps *et al.*, 1992). Red lines show well control. Active oblique-reverse faults thrust early-Cenozoic and older rocks (red/blue) over relatively undeformed Plio-Pleistocene and younger sediments (yellow/orange). Note the rotated and nonplanar geometry of both faults. Possible landslide responsible for the shallow, thrust-nappe 3D geometry of San Cayetano fault is shown. Red, Sespe Formation (~30 Ma); yellow, Upper Saugus Formation (~0.5 Ma); gray, Rincon shale (possible location of inferred slide surface).

terpretation of the seismic-reflection data alone. The seismic and offshore well data clearly document a nonplanar, rotated fault geometry (similar to the shallow Oak Ridge fault shown in Fig. 2), as well as apparent vertical separation and changes in stratigraphy across the Oak Ridge fault at depth. In addition, a prominent unconformity is present south of the fault (that cuts out Sisquoc Formation, green) that is not present north of the fault. This unconformity is now buried and tilts north, indicating a prior history of uplift and erosion, followed by subsidence and basinward tilting of the hanging-wall block.

Stratigraphic Reference Horizons and the Regional Pattern of Uplift and Subsidence

Besides providing important geologic and geophysical constraints on the location and geometry of active subsurface faults, the combined, integrated dataset can also provide critical information on the distribution of regional finite strain in space and time. This is done by correlating and mapping in 3D various stratigraphic reference horizons. Figure 5 shows an example of one such 3D surface that represents a unique time horizon originally mapped by Yeats (1981), and further modified and extended offshore by Sorlien and Kamerling (1998). This horizon was deposited in upper-bathyal water depths of about 500 m and is dated at about 1 Ma. In the eastern onshore Ventura basin, this surface is now found at a maximum depth of nearly 3.5 km (corresponding to a net subsidence of 3 km), whereas across the Oak Ridge fault to the south, shortening has uplifted and folded this same surface by nearly 2 km. This corresponds to a net vertical structural relief across the eastern Oak Ridge fault of almost 5 km since 1 Ma (Yeats, 1988).

Structure contour maps of such deformed surfaces (like Fig. 5) can provide quantitative estimates of the cumulative finite strain field absorbed by folding, faulting, and block rotation since deposition, if the surface can be kinematically restored to its presumed, initial undeformed state (e.g., Gratier *et al.*, 1999; Sorlien *et al.*, 2000). If the original paleodepth of deposition is known, then the regional pattern of (absolute) uplift and subsidence also can be determined. Another example of this is shown in Figure 6. This figure represents a 3D perspective of the base Vaqueros structure contour map derived from kinematic modeling of fold geometry and assuming the deformed surface is developable (Thibert *et al.*, 2005). Vaqueros Formation is a shallow marine deposit dated at about 23–24 Ma (Hoffman *et al.*, 2001). Maximum structural relief varies from an absolute subsidence of about 7 km south of the Red Mountain fault (in the deep Ventura basin) to an absolute uplift of over 1 km near Sulphur Mountain.

Analysis of the older base Vaqueros horizon (~24 Ma) is useful as it reflects the cumulative deformation since the initiation of the Pacific-North American plate boundary in this area (Nicholson *et al.*, 1994). This deformation included Miocene oblique extension, large-scale tectonic rotation, and post-Miocene transpression as the plate boundary geometry and plate motion vector changed with time. The onset of the

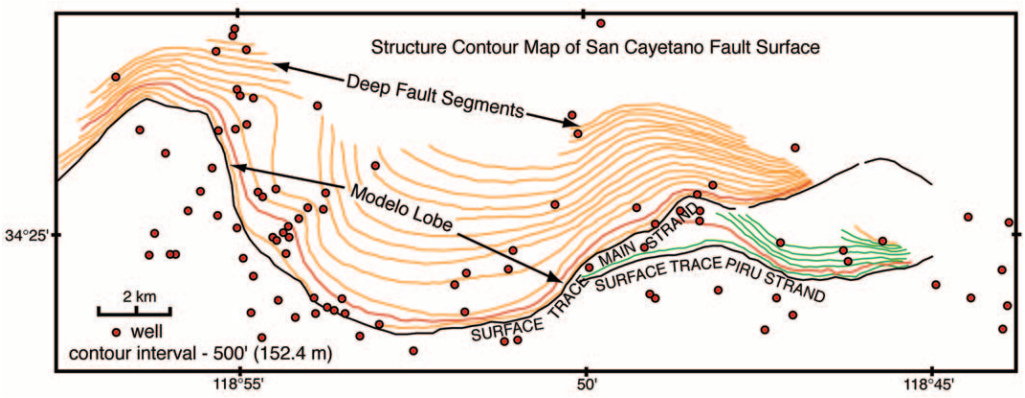

Figure 3. Structure contour map of the San Cayetano fault surface (after Çemen, 1989). Note the unusual lobate shape and shallow dip of the Modelo Lobe segment that extends out in front of the more steeply dipping deep fault segments. Dots show locations of some of the available well control.

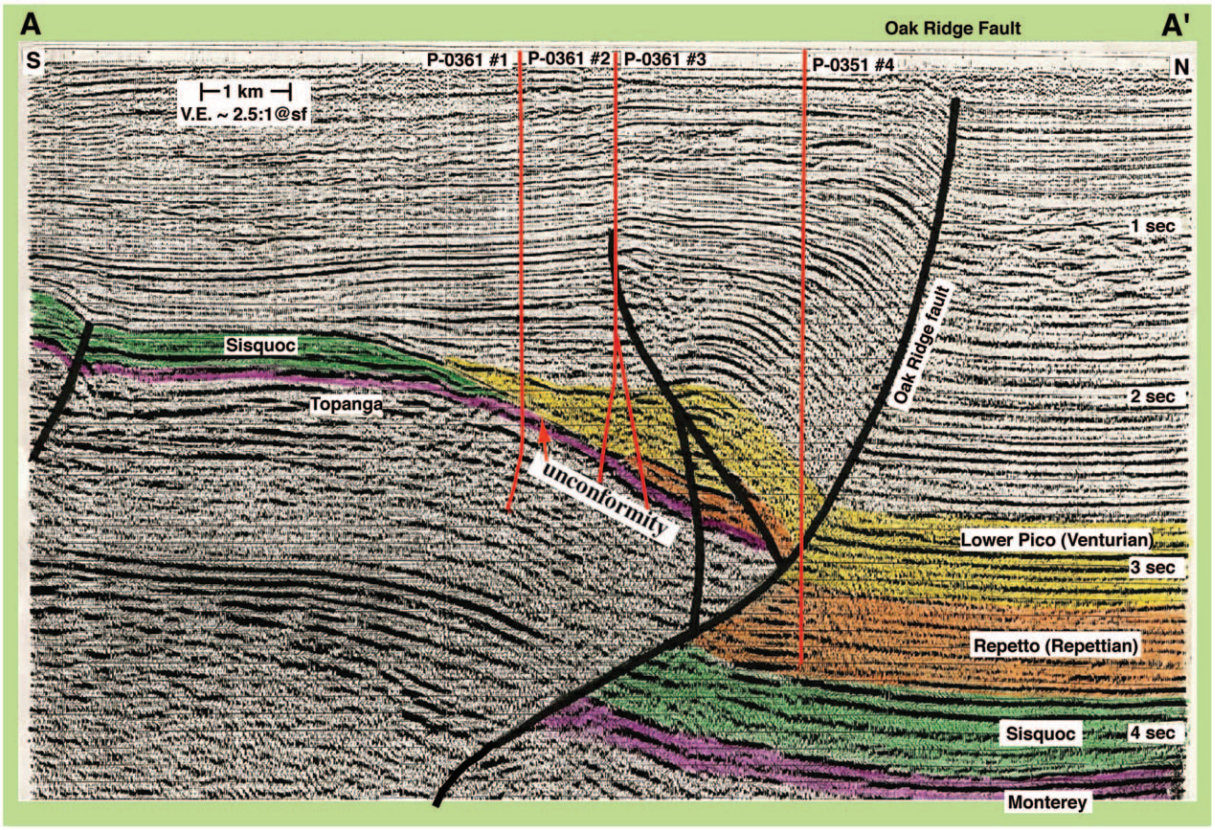

Figure 4. Industry high-fold multichannel seismic reflection profile across the Oak Ridge fault (black lines) in the eastern Santa Barbara Channel showing evidence for uplift, erosion, basinward-tilting, and subsequent subsidence of the hanging-wall (south) block. The Oak Ridge fault is relatively steeply dipping (average dip is 70° or greater) and accommodates left-oblique reverse motion. Note the rotated and nonplanar geometry of the fault, and the tilted unconformity south of the fault that cuts out Sisquoc (green) and lower Repetto (orange) Formations. Red lines show well control.

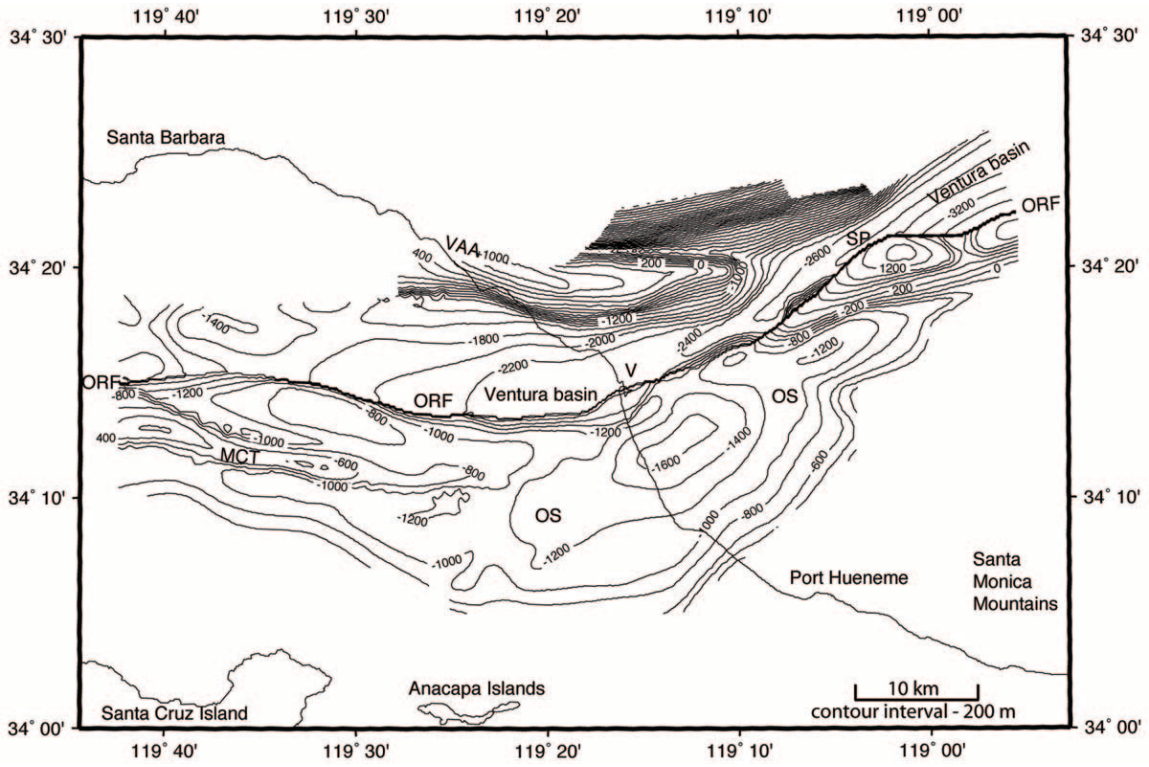

Figure 5. Structure contour map of ~1 Ma horizon mapped by Yeats (1981) and subsequently modified and extended by Sorlien and Kamerling (1998). This horizon was deposited mostly in midbathyal depths of 500–600 m. It documents the cumulative finite strain, as well as the overall regional pattern of uplift and subsidence since deposition. (ORF, Oak Ridge fault; VAA, Ventura Avenue anticline; MCT, Mid-Channel Trend; V, Ventura; OS, Oxnard Shelf; SP, Santa Paula).

more recent transpression, which resulted in folding, basin inversion, and reactivation of normal-separation faults in convergence varied somewhat in space, but was well established in this area by 4–5 Ma (Yeats *et al.*, 1994; Sorlien *et al.*, 1998; Seeber and Sorlien, 2000). Of the 7 km of subsidence documented by the base Vaqueros horizon in the central Ventura basin (Fig. 6), most of this subsidence (up to 5 km) occurred in the last 3 million years or so, with nearly 3 km of subsidence since 1 Ma (Fig. 5) (Yeats, 1981, 1983; Sorlien and Kamerling, 1998). Much of the subsidence and deposition in the northern Los Angeles basin and San Fernando Valley also occurred in Plio-Pleistocene time (Wright, 1991; Yeats, 2001). The bulk of this subsidence thus occurred when the regional deformation was transpressional and thus reflects a crust and mantle response to convergence, and not a feature inherited from an earlier phase of crustal extension (e.g., Yeats, 1983; Niño *et al.*, 1998).

Compaction and Other Possible Nonelastic Effects

Besides faulting, folding, uplift, and subsidence, additional processes may act to absorb finite strain. This includes such nonelastic processes as diagenesis, pressure solution, and compaction (e.g., Dewers and Orteleva, 1990; Deude *et al.*, 2004). In deep, deforming sedimentary basins, these effects can be significant. Figure 7 shows (a) compaction curves (solidity versus depth) for various sedimentary sequences (Baldin and Butler, 1985) including one for the Ventura basin (after McCulloh, 1967); and (b) the relation between percent solidity, percent porosity, and 1D length reductions produced during vertical compaction. Measured porosities in the Ventura basin range from near-surface values of up to 80% to about 20% at depths of ~3 km (Fig. 7a) (e.g., McCulloh, 1967). This corresponds to an overall reduction of 75% in bed thickness, if this reduction in porosity is solely due to vertical (1D) compaction. In the Santa Barbara–Ventura basins, diagenetic compaction can also occur owing to the presence of thick biogenic sediments of the Monterey Formation. The silica in these deposits transforms from noncrystalline Opal A to a more ordered Opal CT, and finally to microcrystalline quartz with increased temperature and pressure from increased depth of burial. Each phase change results in another reduction in porosity of about 25% (Isaacs, 1981). Compaction curves derived from porosity logs in the Ventura basin that penetrate across active faults (e.g., Fig. 8) also suggest that vertical rates of compaction differ between hanging-wall and footwall blocks. Integrated analysis of a typical compaction curve for the deep Ventura basin (e.g., dashed line, Fig. 7a) suggests that such compac-

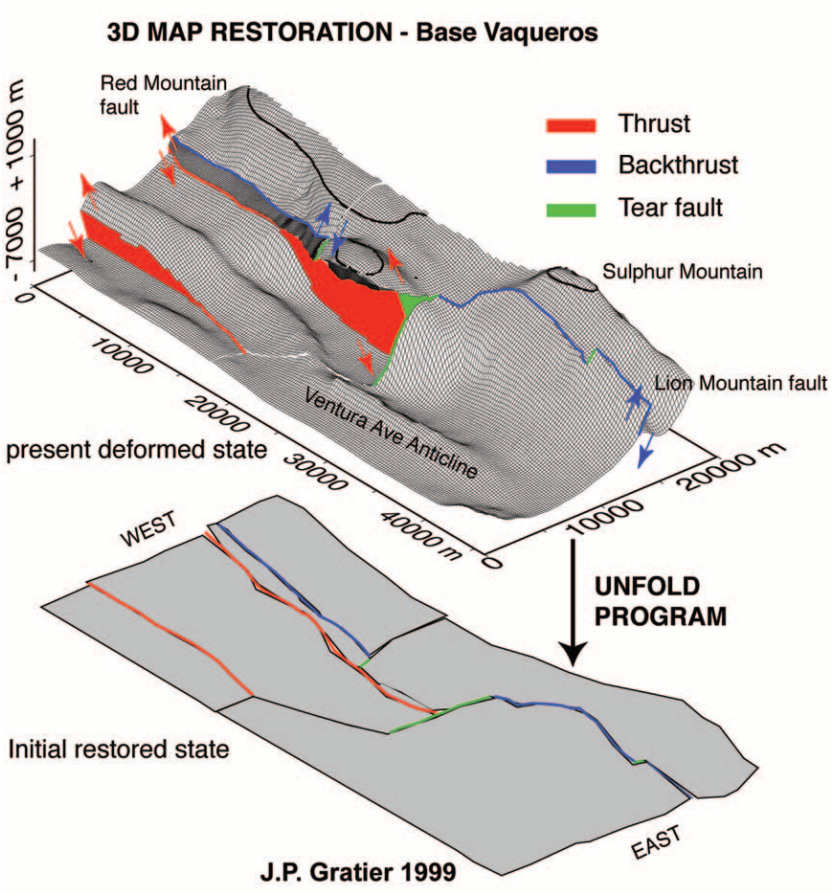

Figure 6. (top) Oblique 3D perspective view of base Vaqueros Formation derived from kinematic modeling of VBSG cross sections (Thibert *et al.*, 2005). View is toward the northwest across the deep Ventura basin and Red Mountain fault. Vaqueros is a ~23–24 Ma shallow marine deposit that has since subsided 7 km in the deep basin. (bottom) 3D map restoration of this developable surface to its initial presumed undeformed state (Thibert *et al.*, 2005). This deformed 3D surface emphasizes that a large part of the regional crustal strain was accommodated by basin subsidence.

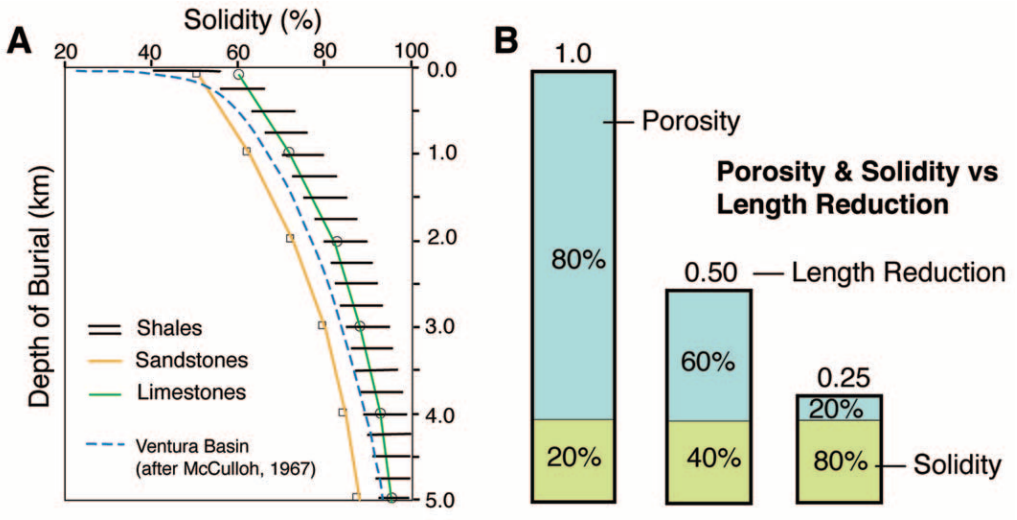

Figure 7. Sediment compaction and its effects on vertical line lengths. (a) Compaction curves (solidity versus depth) for sandstones, limestones, and shales (from Baldwin and Butler, 1985). Dashed line is average compaction curve for the Ventura basin based on porosity well logs (after McCulloh, 1967). (b) Relation between percent solidity (bottom part) versus percent porosity (top part) during vertical (1D) compaction. Ratio at top of each column is the resulting 1D length reduction.

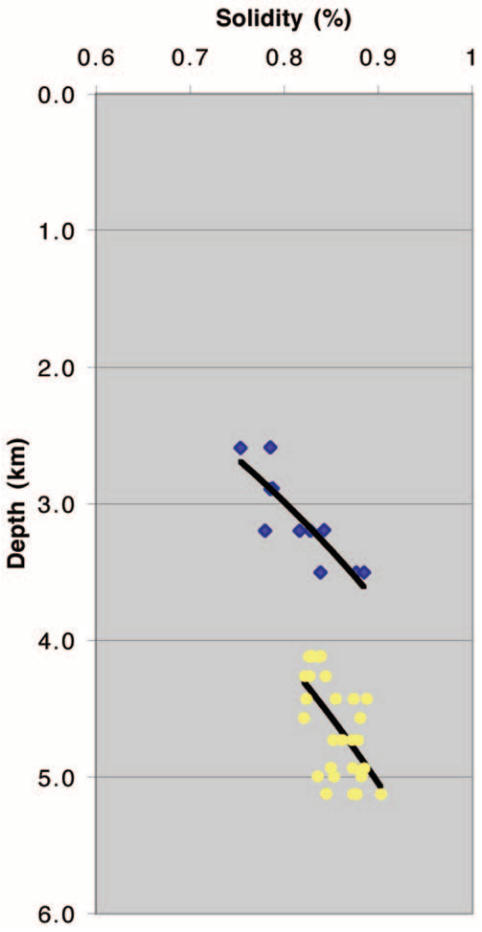

Figure 8. Solidity versus depth in Superior #1 well that penetrates through the Oak Ridge fault. Data show that both sides (diamonds, hanging wall; dots, footwall) of the fault subsided and compacted, followed by uplift of the hanging wall by fault offset (or vice versa). Data also indicate that the rate of compaction differs slightly on the hanging-wall versus footwall side and that fault offset may be less than the observed subsidence.

tion effects may be responsible for as much as 1 km of recent subsidence since 1 Ma (Nicholson *et al.*, 2000).

Results and Implications

A key observation is that much of the observed deformation and subsidence is recent (much of it has occurred since 1 Ma), it is significant (up to 7 km subsidence in the deepest part of the basin), and it strongly influences how geologic and geodetic data should be modeled to infer estimates of regional tectonic strain and fault slip. Moreover, the subsidence has both a local basin component related to nonelastic processes of sediment compaction, diagenesis, pressure solution, and other types of footwall deformation, as well as a much larger regional component related to a lithospheric response to oblique convergence. As such, the subsidence affects a much broader area than just the central Ventura basin.

Studies of the depth to Moho based on analysis of regional seismic phases and teleseismic receiver functions clearly show that Moho is deflected beneath the Ventura basin by about 7–8 km, and this deflection occurs over a much broader wavelength than the basin itself (e.g., Hearn, 1984; Zhu and Kanamori, 2000). As the Moho deflection is similar to the net subsidence of the Vaqueros Formation (Fig. 6), this indicates a mantle component is involved in the process of driving or accommodating the observed regional strain (e.g., Niño *et al.*, 1998). The result is that hanging-wall blocks above basin-bounding faults, such as the Oak Ridge and San Cayetano faults, are also affected by this regional subsidence (Figs. 4 and 8). The implication is that measured rates of rock uplift relative to a reference datum (such as marine terraces relative to paleo-sea level) will underestimate actual rates of structural relief developed by faulting and folding, as hanging-wall uplift must exceed footwall subsidence (and denudation) for any measurable rock uplift relative to the datum to be observed (Pinter *et al.*, 2003).

Another important point is that a significant component of the observed subsidence may be the result of nonelastic processes, such as basin sediment compaction (Fig. 7). Differential compaction across basin-bounding faults (Fig. 8) can produce apparent vertical separation, even in the absence of fault slip. Compaction and subsidence can also cause basin-bounding faults to rotate or "collapse" in toward the basin (Foose, 1973), producing nonplanar faults and surficial motions that mimic deep fault slip (Fig. 9). This is particularly true if the principal stress field is horizontal, as it is in young contractional basins. The nonplanar geometry of the Oak Ridge and San Cayetano faults (Figs. 2 and 4) may be the result of such compaction, shortening, and subsequent fault rotation (Fig. 9). Models for the tectonic evolution of the basin and its associated basin-bounding faults must then be modified to account for these effects. This process of basin sediment compaction is just one of several aseismic or nonelastic mechanisms that may be accommodating crustal strain by footwall deformation.

More importantly, hanging-wall uplift and basin (footwall) compaction and subsidence can increase the potential for gravity sliding toward the basin and the development of additional nonplanar 3D fault geometry. A possible end-member example of this is represented by the eastern (Modelo Lobe) segment of the San Cayetano fault that bounds the eastern Ventura basin. Detailed structure contour maps (Fig. 3) and cross sections (Fig. 2) of the fault surface derived from industry subsurface well data reveal a fault geometry somewhat reminiscent of thrust nappes in the western European Alps (e.g., Lemoine, 1973) and southern Pyrenees (Choukroune and Séguret, 1973). At shallow levels, a large thrust sheet (the Modelo Lobe) with low dip extends out in front of the more steeply dipping fault segment by over 4 km, is nearly 2 km thick, and occupies over

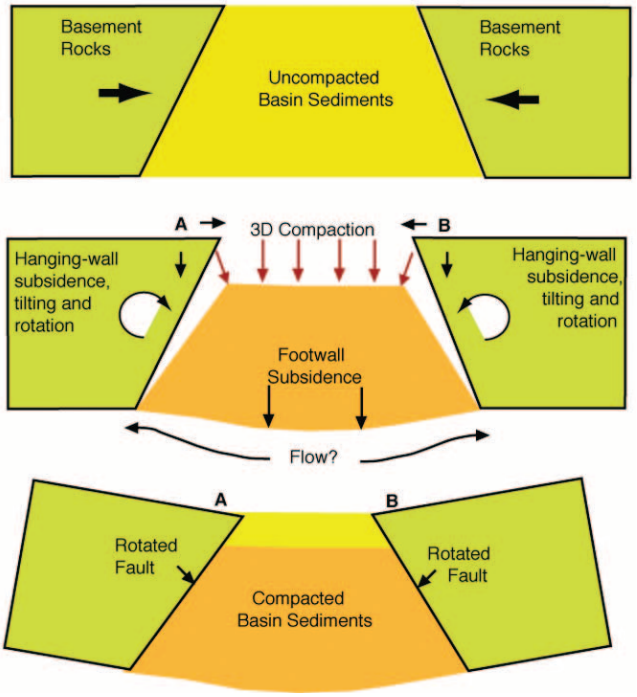

Figure 9. Simple schematic model suggesting how differential basin compaction and isostatic subsidence can produce: (1) apparent vertical separation across faults; (2) surficial displacements (points A and B moving toward each other) that mimic tectonic shortening; (3) tilting and collapse of hanging-wall blocks towards the basin; and (4) fault rotation about horizontal axes. Successive incremental stages of fault rotation with continued basin subsidence and compaction would produce curved, nonplanar fault geometry.

60 cubic km (Fig. 2). This geometry is strongly indicative of deep-seated, gravity-driven failure (e.g., Agliardi *et al.*, 2001) resulting from hanging-wall uplift and subsequent basinward tilting and sliding (or slumping), enhanced by footwall compaction and subsidence.

A simple model that can explain the evolution of this complicated 3D fault geometry is shown in Figure 10. The model involves basically a two-stage process of hanging-wall uplift and basinward tilt due to crustal shortening, fault slip, footwall subsidence, and compaction (Fig. 10e and d), followed by gravity sliding or collapse off the hanging-wall and subsequent fault reactivation which further displaces the slide mass and disrupts the original slide surface (Fig.10c and b). Normal faults can form above the deformed reverse fault (e.g., Fig. 2) due to this gravitational strain within the hanging-wall block. Similar features related to the basinward rotation and collapse of transpressional fault wedges in the hanging-wall are observed above the Hope fault in New Zealand (Eusden *et al.*, 2005). Although alternative models may be used to explain the observed 3D fault geometry, this particular model was chosen to emphasize that some component of downslope movement, slumping, or gravitational collapse (Fig. 10d) must be involved. As such, near-surface displacements on the shallow-dipping Modelo Lobe section of the San Cayetano fault are the result of the release of both accumulated elastic strain energy (from fault slip at depth) and gravitational potential energy (from sliding off the uplifted Topatopa Mountains to the north).

Failure of the mega-slide off the hanging wall and out over the footwall most likely occurred within the Rincon Formation, a ~400-m-thick ductile shale sequence that often accommodates bedding-plane or detachment slip. Where the Rincon Shale accommodates sliding or detachment slip, the angle of internal friction is typically about 15° to 20° (Geo Logic Associates, 2002). The structural dip (toward the basin) of the Rincon, Vaqueros, and Sespe Formations in the hanging wall above the San Cayetano fault is typically about 25° (Fig. 2) (Dibblee, 1990; Hopps *et al.*, 1992). Further reactivation or motion of the slide may have been accommodated by additional shale layers within the Modelo Formation (above the Rincon Shale) and augmented by the presence of overpressured fluids trapped below the base of the slide as a result of continued sediment compaction and overburden loading.

If the model for the evolution of the San Cayetano fault surface is correct (Fig. 10), it predicts that a structural "hole" or "window" should be present just behind the slide where the slide originated. This is, in fact, exactly what is seen. Both topography and geologic surface mapping (Dibblee, 1990) indicate a significant stratigraphic section is missing in the area of the inferred source region (Fig. 11). Behind the slide, Rincon and older rocks (all dipping toward the basin) constitute the only succession present (Figs. 2 and 11). The younger stratigraphic section, mapped elsewhere along strike of the south flank of the Topatopa Mountains, is gone; yet it is precisely this younger section that largely forms the Modelo Lobe of the San Cayetano fault. Further confirmation that the Modelo Lobe is detached is provided by its more "rumpled" appearance (Fig. 11) and its more discordant dips, including tight-to-overturned folds within the Modelo and younger formations (elsewhere within the Modelo Lobe) that are not reflected in the underlying Rincon and older strata (Hopps *et al.*, 1992). The probable reason that this structure was not previously recognized as a mega-slide is because of its large areal extent (~6 km × 5 km), its thickness (~2 km), and the relative coherence of the inferred slide mass. The coherence of the slide mass may also indicate that movement off the hanging wall and out over the footwall (Fig. 10c), may have occurred relatively slowly, and not necessarily as a single, sudden catastrophic collapse.

Regardless of the origin of such unusual 3D fault geometry, gravity sliding can occur whenever sufficient gravitational potential energy is available (e.g., Kehle, 1970). This is particularly true in areas where steep gradients in gravitational potential are produced when dense hanging-wall rocks are uplifted and juxtaposed against the margins of deep, subsiding sedimentary basins across active thrust or oblique-slip faults. Even along strike-slip faults, in areas of restraining bends or stepovers, uplifted material can be dis-

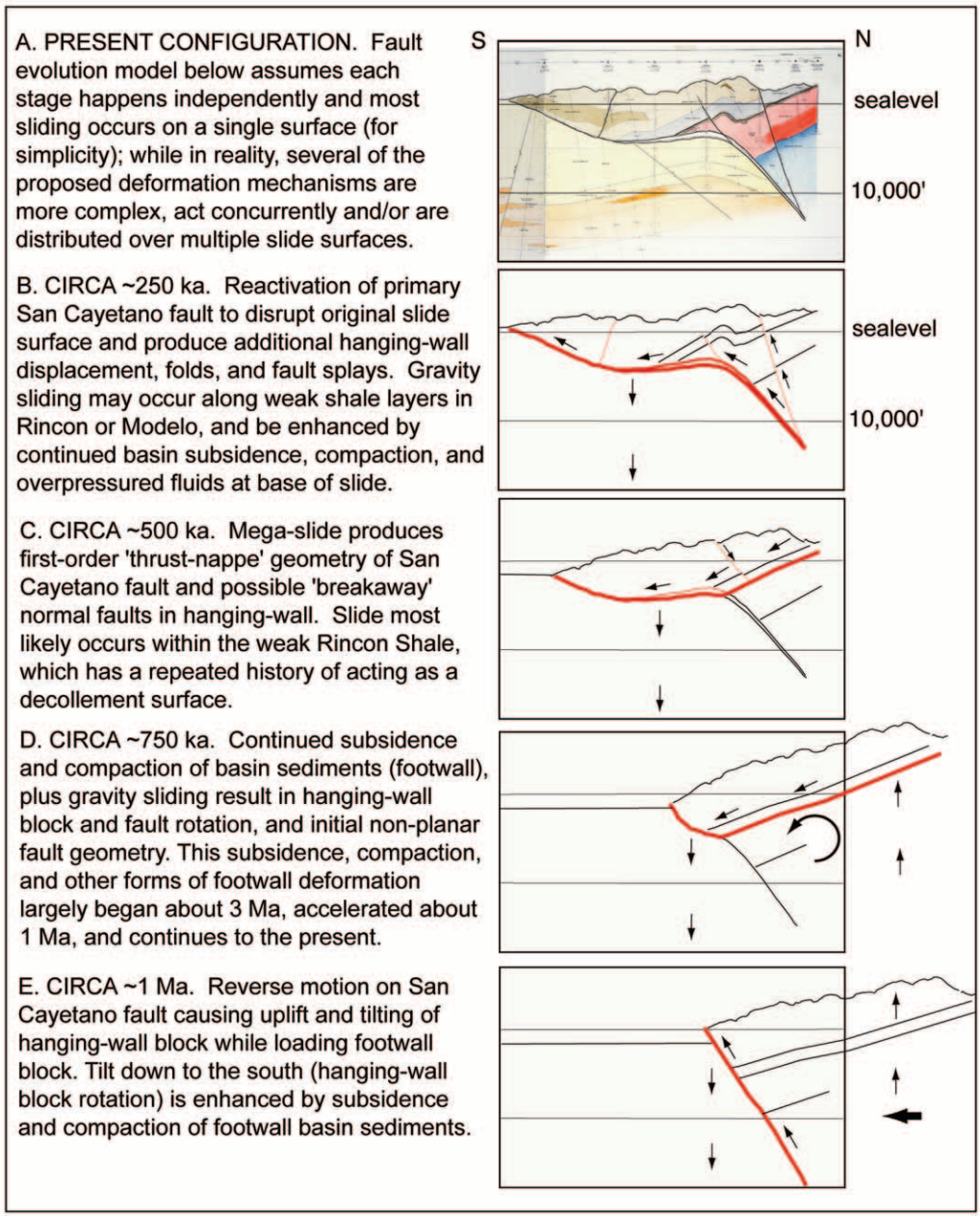

Figure 10. Possible schematic evolution of San Cayetano fault geometry. Initial fault uplift and basin subsidence causes fault and hanging-wall block to rotate and tilt down to south (e). Subsidence, compaction and initial gravity sliding induces collapse and bending of fault surface (d). Mega-slide creates initial thrust-nappe geometry (c). Continued basin subsidence and compaction, along with uplift, folding and fault offset due to continued fault slip disrupts original slide surface, causes continued hanging-wall collapse of fault wedges, and creates present fault geometry (b). Sliding or slumping (on possible multiple slide surfaces) may occur on weak shale layers in the Rincon and Modelo Formations, and may be enhanced by overpressured basin sediments due to compaction and loading, and by continued uplift, shortening, and dynamic slip induced by the fault.

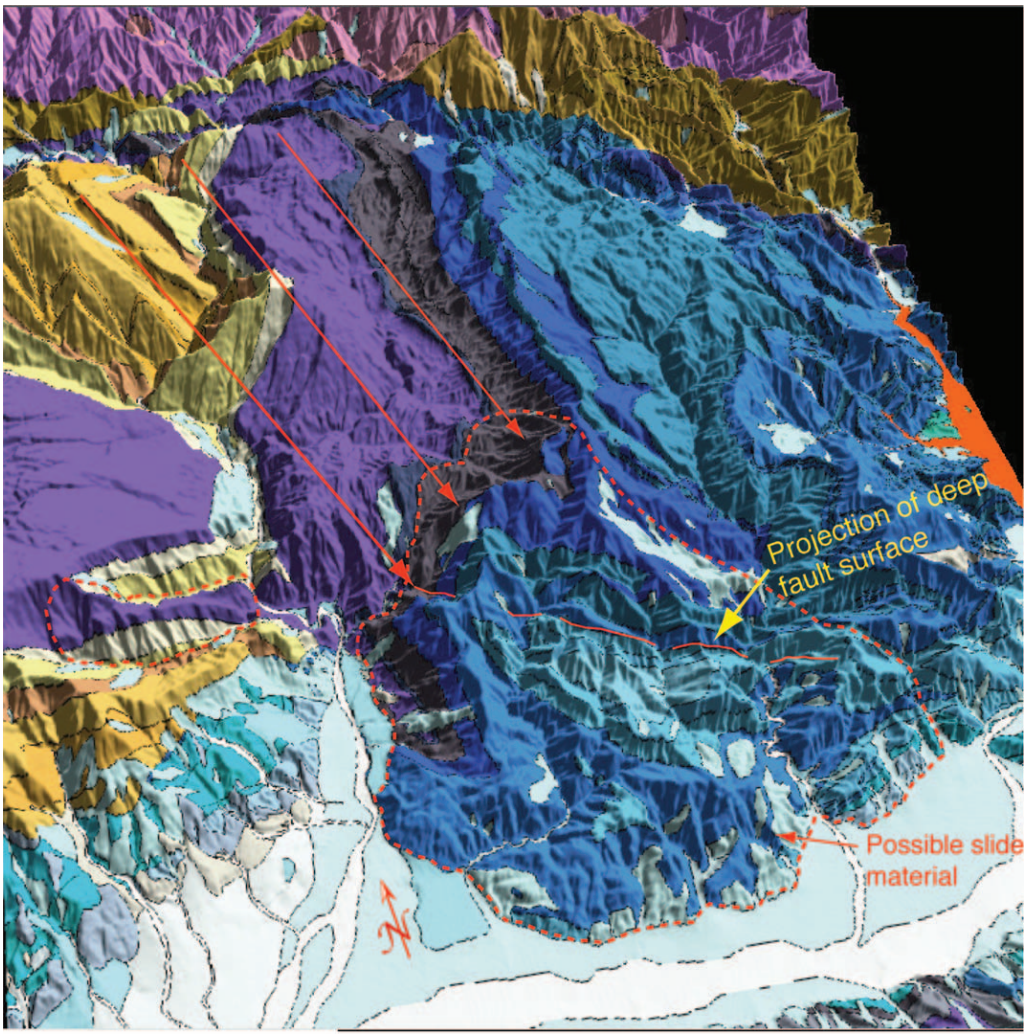

Figure 11. Oblique 3D view looking northeast of DEM overlaid with mapped surface geology (Dibblee, 2002). Note that older (gray, Vaqueros; purple, Sespe; etc.) pre-Rincon Shale rocks (black) are exposed in a window behind the inferred slide material (red dashed line; arrows show possible slide displacement) that exhibits a much more folded, chaotic, and rumpled appearance as a result of slip above a detachment. The inferred slide material extends well out in front of the projected deep San Cayetano fault segment (intermittent solid red line) or the normal range front.

placed across the fault by combinations of thrust faulting and gravity sliding (e.g., Meisling and Weldon, 1986; McClay and Bonora, 2001). Figure 12 shows a diagrammatic map and cross section across the San Andreas fault in the Big Bend area adjacent to the uplifting San Emigdio Mountains (J. C. Crowell, unpublished figure, after Davis, 1978). The fault exhibits a similar 3D geometry to the San Cayetano fault, but on a smaller scale, as a result of oblique-reverse motion, hanging-wall uplift, gravity sliding, and collapse across this convergent section.

Such gravity sliding can be fast or slow. For the San Cayetano fault, if gravity sliding did occur and contributed to the displacement of the large thrust sheet or nappe (e.g., Fig. 10c), this would imply that fault slip measured at the mapped surface trace (e.g., Dolan and Rockwell, 2001) and the high rates of geodetic shortening measured across the basin (e.g., Donnellan *et al.*, 1993) may be related in part to shallow movement or reactivation of the gravity slide, and not solely to large earthquakes at depth or to regional elastic strain accumulation. Furthermore, even if gravity sliding currently does not occur (because the present inferred slide geometry appears rather stable), differential compaction, subsidence, and other possible nonelastic effects in the footwall can still induce both horizontal and vertical motions (Fig. 9) that are also unrelated to either tectonic fault slip or the accumulation of elastic strain.

In terms of seismic hazard, the 3D thrust-nappe geometry of faults like the San Cayetano (Fig. 2) has significant implications for how the fault might behave during dynamic rupture (Fig. 13). Dynamic slip may be inhibited at shallow

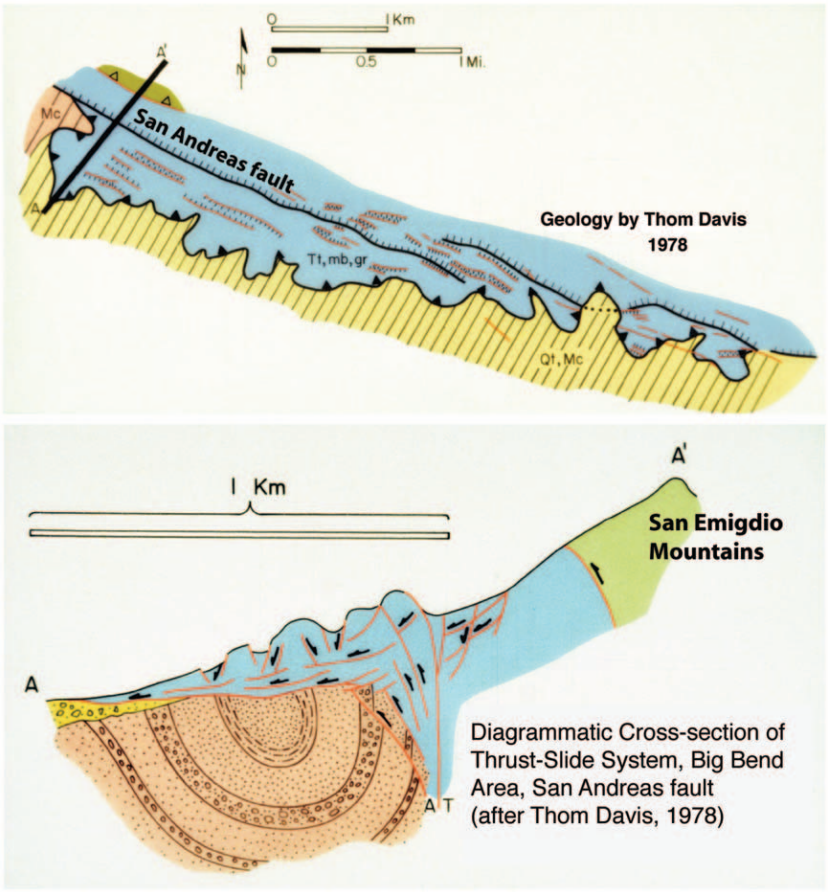

Figure 12. Map (top) and diagrammatic cross section (bottom) across the San Andreas fault in the Big Bend area adjacent to the San Emigdio Mountains (diagram by J. C. Crowell, after Davis, 1978). Cross section shows a similar thrust-nappe geometry as the San Cayetano fault, but on a smaller scale. Fault geometry results from oblique-reverse motion, uplift, and gravity sliding across this convergent section of the strike-slip San Andreas fault.

levels by the presence of the slide and the change in fault dip with depth (Fig. 13b). Large ruptures may reactivate the slide (Fig. 13c), either by dynamic triggering of the weak slide surface or by statically pushing the thrust wedge from behind. Alternatively, the rupture may propagate to the surface along the shallow thrust front (Fig. 13a) or behind the slide (Fig. 13d). However, if the shallow thrust sheet does fail, the slip on the shallow fault segment may or may not be related to tectonic slip on the deep fault segment. If the thrust-nappe geometry is the result of an ancient gravity slide, the slide can be reactivated independent of slip at depth and/or aseismically (Fig. 13e), as long as sufficient gravitational potential energy is available in the system. In either case, observations of near-surface slip or large slip events at the toe of the slide (Dolan and Rockwell, 2001) may not be indicative of tectonic slip or large earthquakes at depth on the fault. Similarly, not all large earthquake ruptures at depth will necessarily result in large, observable slip events at the current mapped surface trace (Fig. 13b and d).

Conclusions

To summarize, across the Ventura and Los Angeles basins, high rates of oblique crustal strain have been measured. Models used to infer the subsurface geometry of active faults—or used to resolve geodetic strain or geologic data into fault slip—typically presume rigid footwall blocks, nondeforming planar fault surfaces, and deformation that is largely restricted to the hanging wall. In California, however, deep, subsiding basins are often bounded by oblique reverse faults that thrust early-Cenozoic and older rocks over young unconsolidated sediments (Fig. 2). This suggests that compaction, subsidence, gravity sliding, and other types of nonelastic deformation may play an important role in accommodating regional tectonic strain (e.g., Fig. 10). Even in the absence of active crustal shortening, sediment compaction alone can produce surficial motions that mimic deep fault slip (Fig. 9). This implies that inferred slip rates and the derived seismic hazard can be under- or overestimated depending on what model assumptions are made. In the presence of regional isostatic subsidence, reference to sea level or paleo-sea level can underestimate the rate of tectonic uplift (and thus fault slip), if this subsidence is ignored (Pinter *et al.*, 2003). On the other hand, subsidence, compaction, pressure solution, and diagenesis of footwall sediments, plus basinward gravity sliding of hanging-wall rocks can lead to increased vertical separation, fault rotation, and horizontal motion (Figs. 9 and 10), even in the absence of active fault slip at depth or elastic strain accumulation. Such effects would contribute to horizontal and vertical motions in both geologic and geodetic data, resulting in overestimates of the inferred seismic hazard.

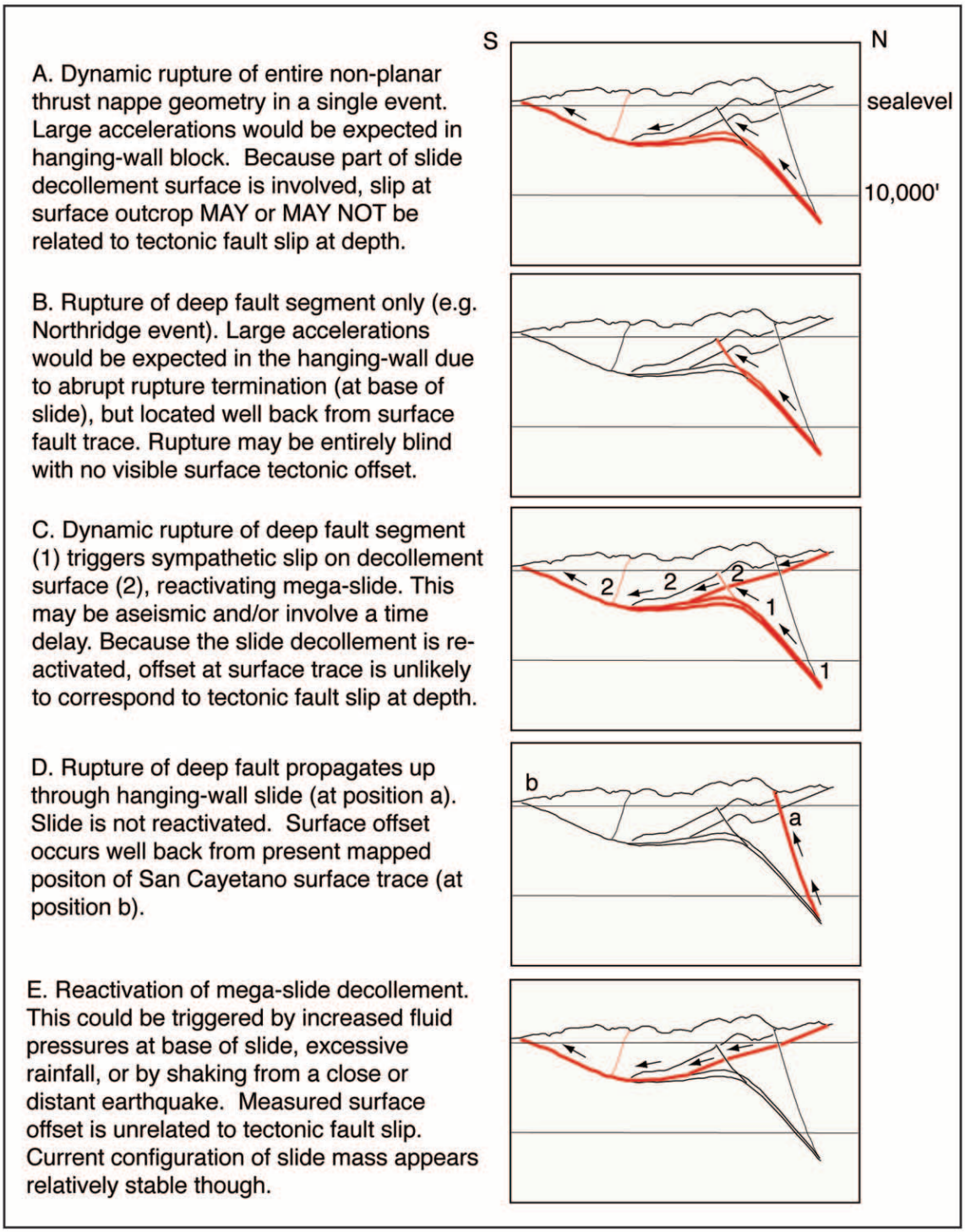

Figure 13. Possible rupture scenarios of the San Cayetano fault. Only "a" involves coseismic fault rupture up to the current mapped surface trace. Others are either blind (b), involve rupture through the hanging wall (d), or involve reactivation of the inferred slide mass (e.g., c and e). Note that because gravity-driven failure may be involved even in "a" (if gravitational potential energy is still available in the system), surface slip may not be related to slip at depth on the deep fault segment.

The observed 3D geometry of active basin-bounding faults also implies that additional care should be taken in extrapolating near-surface measurements or estimates of fault slip and dip to seismogenic depths. Dynamic rupture models may also need to be modified to allow for a wider range of possible rupture scenarios (Fig. 13) given the dramatic 3D structure of some basin-bounding faults and the various processes, tectonic events, and variations in material properties that led to its development.

Acknowledgments

We are indebted to Jim Brune for numerous discussions and encouragement to pursue this subject. Jarg Pettinga and Tom Rockwell provided critical and constructive reviews that substantially improved the manuscript. Additional reviews were provided by Ruth Harris and Michael Fisher. We thank John Crowell for permission to use his unpublished diagram shown in Figure 12 and Dave Valentine for assistance with the geologic overlay shown in Figure 11. This work was supported in part by several grants, including awards from the National Science Foundation, the U.S. Geological Survey NEHRP, and the Southern California Earthquake Center (SCEC). SCEC contribution number 1046.

References

Argliardi, F., G. B. Crosta, and A. Zanchi (2001). Structural constraints on deep-seated slope deformation kinematics, *Eng. Geol.* **59,** no. 1–2, 83–102.

Argus, D. F., M. B. Heflin, A. Donnellan, F. H. Webb, D. Dong, K. J. Hurst, D. C. Jefferson, G. A. Lyzenga, M. M. Watkins, and J. F. Zumberge (1999). Shortening and thickening of metropolitan Los Angeles measured and inferred by using geodesy, *Geology* **27,** 703–706.

Argus, D. F., M. B. Heflin, G. Peltzer, F. Crampé, and F. H. Webb (2005). Interseismic strain accumulation and anthropogenic motion in metropolitan Los Angeles, *J. Geophys. Res.* **110,** no. B4, B04401, doi 10.1029/2003JB002932.

Baldwin, B., and C. O. Butler (1985). Compaction curves, *Am. Assoc. Petrol. Geol. Bull.* **69,** 622–626.

Bawden, G. W., W. Thatcher, R. S. Stein, K. W. Hudnut, and G. Peltzer (2001). Tectonic contraction across Los Angeles after removal of groundwater pumping effects, *Nature* **412,** 812–815.

Çemen, I. (1989). Near surface expression of the eastern part of the San Cayetano fault: a potentially active thrust fault in the California Transverse Ranges, *J. Geophys. Res.* **94,** no. B7, 9665–9677.

Childs, J. R., and P. E. Hart (2004). National archive of marine seismic surveys (NAMSS): U.S. Geological Survey program to provide new access to proprietary data, *EOS Trans. AGU* **85,** no. 47, NG43A-0441.

Choukroune, P., and M. Séguret (1973). Tectonics of the Pyrenees: role of compression and gravity, in *Gravity & Tectonics*, K. E. DeJong and R. Scholten (Editors), John Wiley & Sons, New York, 141–156.

Davis, T. L. (1978). Quaternary tectonics along the Big Bend segment of the San Andreas fault zone, California, *Geol. Soc. Am. Abstr. Programs* **10,** no. 3, 102.

Dibblee, T. W., Jr. (1990). Geologic Maps of the Fillmore and Piru Quadrangles, 1:24,000, Dibblee Geological Foundation, Santa Barbara, California.

Dibblee, T. W., Jr. (2002). CD-3: geology of the Ventura area and eastern Santa Ynez Mountains, 1:24,000, Dibblee Geological Foundation, digital geo-referenced copies of 16 maps and 17 quadrangles.

Deude, V., L. Dormieux, S. Maghous, J. F. Barthelemy, and D. Bernaud (2004). Compaction process in sedimentary basins: the role of stiffness increase and hardening induced by large plastic strains, *Int. J. Numerical Anal. Methods Geomechan* **28,** no. 13, 1279–1303.

Dewers, T., and P. Ortoleva (1990). Interaction of reaction, mass transport, rock deformation during diagenesis: mathematical modeling of intergranular pressure solution, stylolites, and differential compaction cementation, in *Prediction of Reservoir Quality*, I. D. Meshri and P. J. Orteleva (Editors), AAPG Memoir 49, 21,285–21,297.

Dolan, J. F., and T. Rockwell (2001). Paleoseismic evidence for a very large (Mw >7), post-A.D. 1660 surface rupture on the eastern San Cayetano Fault, Ventura County, California: was this the elusive source of the damaging 21 December 1812 earthquake? *Bull. Seism. Soc. Am.* **91,** no. 6, 1417–1432.

Dolan, J. F., K. E. Sieh, T. K. Rockwell, R. S. Yeats, J. Shaw, J. Suppe, G. J. Huftile, and E. M. Gath (1995). Prospects for larger or more frequent earthquakes in the Los Angeles metropolitan region, *Science* **267,** 199–205.

Donnellan, A., B. H. Hager, R. W. King, and T. A. Herring (1993). Geodetic measurement of deformation in the Ventura Basin region, southern California, *J. Geophys. Res.* **98,** 21,727–21,739.

Eusden, J. D., Jr., J. R. Pettinga, and J. K. Campbell (2005). Structural collapse of a transpressional hanging-wall fault wedge, Charwell region of the Hope fault, South Island, New Zealand, *N. Z. J. Geo. Geophys.* **48,** 295–309.

Foose, R. M. (1973). Vertical tectonism and gravity in the Big Horn Basin and surounding ranges of the Middle Rocky Mountains, in *Gravity & Tectonics*, K. E. DeJong and R. Scholten (Editors), John Wiley & Sons, New York, 443–455.

GeoLogic Associates, Geotechnical Investigation, Proposed Landfill Expansion, Tajiguas Sanitary Landfill, Santa Barbara County, California, 2002.

Gratier, J.-P., T. Hopps, C. C. Sorlien, and T. Wright (1999). Recent crustal deformation in southern California deduced from the restoration of folded and faulted strata, *J. Geophys. Res.* **104,** 4887–4899.

Hager, B. H., G. A. Lyzenga, A. Donnellan, and D. Dong (1999). Reconciling rapid strain accumulation with deep seismogenic fault planes in the Ventura Basin, California, *J. Geophys. Res.* **104,** no. 11, 25,207–25,219.

Hearn, T. M. (1984). Pn travel times in Southern California, *J. Geophys. Res.* **89,** no. B3, 1843–1855.

Hoffman, J., D. R. Prothero, and L. L. Donohoo (2001). Magnetic stratigraphy of the Oliogocene-Miocene Vaqueros formation and Molluscan stage, California, *Cordilleran Section — Geol. Soc. Am. and Pacific Section Am. Assoc. Petrol. Geol. Abstracts with Programs*, **33,** no. 3, A-60.

Hopps, T. E., H. E. Stark, and R. J. Hindle (1992). Subsurface geology of Ventura Basin, California, Ventura Basin Study Group Report, 45 pp., 17 structure contour maps and 84 structure panels comprising 21 cross sections, Rancho Energy Consultants, Inc., Santa Paula, California.

Howard, J. (1988). Sedimentation of the Sespe Formation in southern California, in *Santa Barbara and Ventura Basins: Tectonics, Structure, Sedimentation, Oilfields Along an East-West Transect*, A. G. Sylvester and G. C. Brown (Editors), Coast Geological Society Field Guide No. 64, 53–69.

Huftile, G., and R. S. Yeats (1995). Convergence rates across a displacement transfer zone in the western Transverse Ranges, Ventura basin, California, *J. Geophys. Res.* **100,** 2043–2068.

Isaacs, C. M. (1981). Porosity reduction during diagenesis of the Monterey Formation, Santa Barbara coastal area, California, in *The Monterey Formation and Related Siliceous Rocks of California*, R. E. Garrison, *et al.* (Editors), Pacific Section SEPM, Los Angeles, California, 257–271.

Kamerling, M., and C. Nicholson (1996). The Oak Ridge fault and fold system, Eastern Santa Barbara Channel, California, 1995 SCEC Annual Report, Vol. 2, C26–C30.

Kehle, R. O. (1970). Analysis of gravity sliding and orogenic translation, *Geol. Soc. Am. Bull.* **81,** 1641–1664.

Larsen, S. C., D. C. Agnew, and B. H. Hager (1993). Strain accumulation in the Santa Barbara Channel: 1970–1988, *J. Geophys. Res.* **98,** no. 2, 2119–2133.

Lemoine, M. (1973). About gravity gliding tectonics in the Western Alps, in *Gravity & Tectonics*, K. E. DeJong and R. Scholten (Editors), John Wiley & Sons, New York, 201–215.

McClay, K., and M. Bonora (2001). Analog models of restraining stepovers in strike-slip fault systems, *Am. Assoc. Petrol. Geol. Bull.* **85,** no. 2, 233–260.

McCulloh, T. H. (1967). Mass properties of sedimentary rocks and gravimetric effects of petroleum and natural-gas reservoirs, *U.S. Geol. Surv. Profess. Pap. 528-A*, 50 pp. plus plates.

Meisling, K. E., and R. J. Weldon (1986). Cenozoic uplift of the San Bernardino Mountains: possible thrusting across the San Andreas fault, *Geol. Soc. Am. Abstracts with Programs* **18,** no. 2, 157.

Namson, J., and T. L. Davis (1991). Detection and seismic potential of blind trusts in the Los Angeles, Ventura, and Santa Barbara areas, and adjoining Transverse Ranges, *U.S. Geol. Surv. Final Technical Report*.

Nicholson, C., and M. J. Kamerling (1998). Reliability of 2D kinematic fold models to infer deep fault structure in the western Transverse Ranges, California, in *Proceedings of the NEHRP Conference and Workshop on the Northridge, California Earthquake*, Vol. II, 299–306.

Nicholson, C., and M. J. Kamerling (1999). Acquisition of 3D subsurface well data analyses and 3D GIS for the Ventura Basin, California, *U.S. Geol. Surv. Final Tech. Rept.*, 19 pp.

Nicholson, C., C. C. Sorlien, T. Atwater, J. C. Crowell, and B. P. Luyendyk (1994). Microplate capture, rotation of the western transverse ranges and initiation of the San Andreas transform as a low-angle fault system, *Geology* **22,** 491–495.

Nicholson, C., C. C. Sorlien, M. J. Kamerling, J.-P. Gratier, and L. Seeber (2000). Influence of active subsidence, compaction, and footwall defomation on estimates of fault slip, geodetic strain, and seismic hazard, *EOS Trans. AGU* **81,** no. 48, F1213.

Niño, F., J. Chéry, and J.-P. Gratier (1998). Mechanical modeling of compressional basins: origin and interaction of faults, erosion, and subsidence in the Ventura basin, California, *Tectonics* **17,** no. 6, 955–972.

Ogle, B. A., W. S. Wallis, R. G. Heck, and E. B. Edwards (1987). Petroleum geology of the Monterey Formation in the offshore Santa Maria/Santa Barbara areas, in *Cenozoic Basin Development of Coastal California*, R. V. Ingersoll and W. G. Ernst (Editors), Prentice-Hall, Englewood Cliffs, New Jersey, 382–406.

Pinter, N., C. C. Sorlien, and A. T. Scott (2003). Fault-related fold growth and isostatic subsidence, California Channel Islands, *Am. J. Sci.* **303,** 300–318.

Redin, T., J. Forman, and M. J. Kamerling (1998). Regional structure cross section across the eastern Santa Barbara Channel, from eastern Santa Cruz Island to the Carpinteria area, Santa Ynez Mountains, in *Structure and Petroleum Geology, Santa Barbara Channel, California*, D. S. Kunitomi, T. E. Hopps, and J. M. Galloway (Editors), Bakersfield, California Pacific Section AAPG MP-46, 195–197, plate 3.

Redin, T., J. Forman, and M. J. Kamerling (2005). Santa Barbara Channel structure and correlation sections, Pacific Section AAPG Cross Sections CS-32 through CS-42, Bakersfield, California.

Seeber, L., and C. C. Sorlien (2000). Listric thrusts in the western Transverse Ranges, California, *Geol. Soc. Am. Bull.* **112,** 1067–1079.

Shaw, J. H., and J. Suppe (1994). Active faulting and growth folding in the eastern Santa Barbara Channel, California, *Geol. Soc. Am. Bull.* **106,** 607–626.

Shaw, J. H., and J. Suppe (1996). Earthquake hazards of active blind-thrust faults under the central Los Angeles basin, California, *J. Geophys. Res.* **101,** 8623–8642.

Sorlien, C. C., and M. J. Kamerling (1998). Fault displacement and fold contraction estimated from unfolding of Quaternary strata onshore and offshore Ventura basin, California, *U.S. Geol. Surv. NEHRP Final Technical Report 97-GR-03085*, 16 pp., digital map scale 1/100,000.

Sorlien, C. C., J-P Gratier, B. P. Luyendyk, J. S. Hornafius, and T. E. Hopps (2000). Map restoration of folded and faulted late Cenozoic strata across the Oak Ridge fault, onshore and offshore Ventura basin, California, *Geol. Soc. Am. Bull.* **112,** no. 7, 1080–1090.

Sorlien, C. C., E. H. McWayne, M. J. Kamerling, and J. Galloway (1998). Late Cenozoic faulting and progressive folding of northern Santa Rosa Island and southwestern Santa Barbara Channel, California, in *Structure and Petroleum Geology, Santa Barbara Channel, California*, D. S. Kunitomi, T. E. Hopps, and J. M. Galloway (Editors), Pacific Section AAPG Misc. Publ. MP-46, 121–141.

Suppe, J., and D. A. Medwedeff (1990). Geometry and kinematics of fault-propagation folding, *Eclogae Geol. Helv.* **83,** no. 3, 409–454.

Thibert, B., J.-P. Gratier, and J.-M. Morvan (2005). A direct method for modeling and unfolding developable surfaces and its application to the Ventura Basin (California), *J. Struct. Geol.* **27,** 303–316.

U.S. Geological Survey (1998). *A Plan for Implementing a Real-Time Seismic Hazard Warning System*, A Report to Congress, 33 pp.

Wright, T. L. (1991). Structural geology and tectonic evolution of the Los Angeles basin, California, in *Active Margin Basins*, K. T. Biddle (Editor), AAPG Memoir 52, 35–134.

Yeats, R. S. (1981). Deformation of a 1 Ma datum, Ventura basin, *U.S. Geol. Surv. Final Rept.* 27 pp.

Yeats, R. S. (1983). Large-scale Quaternary detachments in Ventura basin, Southern California, *J. Geophys. Res.* **88,** no. B1, 569–584.

Yeats, R. S. (1988). Late Quaternary slip rate on the Oak Ridge Fault, Transverse Ranges, California: implications for seismic risk, *J. Geophys. Res.* **93,** 12,137–12,149.

Yeats, R. S. (1993). Converging more slowly, *Nature* **366,** 299–301.

Yeats, R. S. (2001). Neogene tectonics of the East Ventura and San Fernando Basins, California: an overview, in *Geology and Tectonics of the San Fernando Valley and East Ventura Basin, California*, T. L. Wright and R. S. Yeats (Editors), Pacific Section AAPG Guidebook GB-77, 9–36.

Yeats, R. S., and G. J. Huftile (1995). Oak Ridge fault system and the 1994 Northridge, California, earthquake, *Nature* **373,** 418–420.

Yeats, R. S., G. J. Huftile, and L. T. Sitt (1994). Late Cenozoic tectonics of the east Ventura basin, California, *Am. Asoc. Petrol. Geol. Bull.* **78,** 1040–1074.

Zhu, L., and H. Kanamori (2000). Moho depth variation in Southern California from teleseismic receiver functions, *J. Geophys. Res.* **105,** no. 2, 2969–2980.

Laboratoire de Géophysique Interne et Tectonophysique
Université Joseph Fourier
38041 Grenoble, France
(J.-P.G.)

Rancho Energy, Inc.
Ventura, California 93001
(T.E.H.)

Venoco, Inc.
Carpenteria, California 93013
(M.J.K.)

Marine Science Institute
University of California
Santa Barbara, California 93106
(C.N.)

Institute for Crustal Studies
University of California
Santa Barbara, California 93106
(C.C.S.)

Manuscript received 6 November 2006.